Analytical Creeping Waves Model at 60 GHz for Off-Body Communications

Theodoros Mavridis*†, Luca Petrillo*, Julien Sarrazin†,
David Lautru†, Aziz Benlarbi-Delaï†, and Philippe De Doncker*

*OPERA WCG Dpt., Polytechnic School of Brussels Université Libre de Bruxelles, B-1050 Brussels,
Email: tmavridi@ulb.ac.be ; lpetrillo@ulb.ac.be ; pdeonck@ulb.ac.be
†UPMC Univ Paris 06, UR2, L2E, F-75005, Paris, France,
Email: julien.sarrazin@upmc.fr ; david.lautru@upmc.fr ; aziz.benlarbi_delaï@upmc.fr

***Abstract*—In the field of 60 GHz high data rate wireless and Body Area Networks communications a fast computation and accurate analytical model for creeping waves is described in this paper. The scattering of a plane wave by a perfectly conducting cylinder (PEC) is presented. It is shown that at 60 GHz higher creeping waves modes can be neglected. The model is then compared with experimental results.**

***Index Terms*—Off-Body, BAN's, cylinder scattering, millimeter wave communication, 60 GHz, creeping waves, ray-tracing**

I. Introduction

The popularity of wireless communication technologies has increased the need for reliable, high-speed communications. To cope with the need for high-data rate transmission, new technologies have been proposed that use ultra wide bands (UWB) of the RF spectrum, such as 60 GHz communications. This band seems to be an efficient solution to realize indoor communication with data rates of a few Gbit/s [1]. The progress in low-cost mm-wave circuit design, but also in miniaturization, makes 60 GHz communications a good candidate for Body Area Networks (BANs) (off- and on-body communications) [2], [3]. To allow the development of 60 GHz BANs communication, the total field around the human body has to be modeled. In this paper, a ray-tracing propagation model around a cylinder body is presented.

In this paper, the calculation of the scattering of a plane wave by a convex cylinder at 60 GHz is studied. A propagation model is proposed based on UTD results [6], [7], [8]. Simplifications of the UTD solution can be made because the shadow boundary width, as introduced by [6], can be neglected. The model proposed here only calculates the asymptotic solutions in the lit and shadow regions.

This article summarizes the results of our fast computation Off-Body model represented by a PEC cylinder. A special interest is given on the creeping wave solutions. Section II presents the equation of a plane wave diffracted by a PEC cylinder for both TM and TE cylinder. A simplified Off-Body model is also presented to allow a faster computation. Section III shows simulations which verify the model developed. The experimental validations of the creeping wave path loss are shown in Section IV. Finally, Section V concludes the paper.

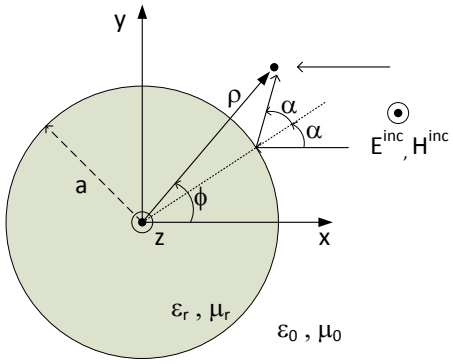

Fig. 1. Geometry

II. Diffracted Wave Equations

A. Problem Definition

The human body is modelled as an PEC infinite cylinder with a radius a, a relative permittivity ε_r, the vacuum permeability and a principal axis $\hat{z}$. The scattering of a TM plane wave on it is studied. The incident plane wave have equation is :

$$\mathbf{E}^{\text{inc}} = e^{jk_0 x}\hat{z} \tag{1}$$

In this paper, the electric field is noted as a scalar quantity :

$$E_z^{\text{inc}} = e^{jk_0 x} \tag{2}$$

where k_0 is the wave number and x is the Cartesian abscissa as shown in fig. 1. The TE plane wave is given by the scalar magnetic field

$$H_z^{\text{inc}} = e^{jk_0 x} \tag{3}$$

B. TM polarization

The total field is given by the sum of the incident field and the scattered field developed in cylindrical series [4] with the polar coordinates system (ρ, ϕ).

$$E_z^{\text{tot}} = \sum_{n=-\infty}^{\infty} j^{-n}\{J_n(k_0\rho) + a_n H_n^{(2)}(k_0\rho)\}e^{-jn\phi} \quad (4)$$

and the boundary condition on a general dielectric cylinder gives [4] by introducing $k_1 = k_0\sqrt{\epsilon_r\mu_r}$:

$$a_n = \frac{J_n'(k_0a)J_n(k_1a) - \sqrt{\varepsilon_r/\mu_r}J_n(k_0a)J_n'(k_1a)}{\sqrt{\varepsilon_r/\mu_r}J_n'(k_1a)H_n^{(2)}(k_0a) - J_n(k_1a)H_n^{(2)'}(k_0a)} \quad (5)$$

In a perfect electromagnetic conducting (PEC) cylinder, the boundary condition is easier to compute :

$$a_n = -\frac{J_n(ka)}{H_n^{(2)}(ka)} \quad (6)$$

where $k = k_0$. In those equations, Bessel's functions $J_n(x)$ and second kind Hankel functions $H_n^{(2)}(x)$ are introduced [5].

The sum in equation (4) is complicated to compute quickly and do not have any physical meaning. In the lit region introduced by [6], the total field can be calculated by the Geometrical Optics (GO) with accuracy. The shadow region is calculated thanks to a creeping wave formulation.

1) Lit Region: In the lit region ($\phi < \pi/2$), the total field can be obtained by a sum of the incident wave and a reflected one [11].

$$E_z^{\text{tot}} = e^{jk\rho\cos\phi} - e^{jka\cos\alpha}e^{-jks_r}\sqrt{\frac{\rho_r}{\rho_r + s_r}} \quad (7)$$

where $\rho_r = \frac{a}{2}\cos\alpha$, α is the reflection angle and s_r is the travelled distance between the reflection position and the observation one.

2) Shadow Region: To define the creeping waves which appear in the shadow region, the use of Watson transformation is required. The total electric field (4) in the shadow region ($\phi > \pi/2$) becomes:

$$E_z^{\text{tot}} = 2\pi\sum_s j^{\upsilon_s}\frac{J_{\upsilon_s}(ka)}{H_{\upsilon_s}^{(2)}(ka)}H_{\upsilon_s}^{(2)}(k\rho)\Phi_{\upsilon_s}(\phi) \quad (8)$$

with $\Phi_\upsilon(\phi) = \frac{\cos\upsilon(\phi-\pi)}{\sin\upsilon\pi}$ and $\upsilon_s = ka + m\tau_s$. In those equations, $m = (ka/2)^{1/3}$ and τ_s satisfies:

$$W_2(\tau_s) = 0. \quad (9)$$

The function $W_2(x)$ is defined as a second kind Airy's function $A(x)$ [6] as following : $W_2(z) = 2e^{j\pi/6}\sqrt{\pi}A(e^{j4\pi/3}z)$. This solution can be interpreted as the creeping wave modes. At 60 GHz, it can be shown that the first mode is predominant. It can be shown also that in this case: $\Phi_{\upsilon_s}(\phi) \simeq je^{-j\upsilon_s\phi}$. This allows us to obtain the creeping wave equation for the total electric field around a PEC cylinder:

$$E_z^{\text{tot}} \simeq 2\pi j^{\upsilon_1+1}\frac{J_{\upsilon_1}(ka)}{H_{\upsilon_1}^{(2)}(ka)}H_{\upsilon_1}^{(2)}(k\rho)e^{-j\upsilon_s\phi} \quad (10)$$

The calculation of complex order Bessel's functions is not trivial and not necessary if $\rho \simeq a$ it can be shown that:

$$E_z^{\text{tot}} \simeq 2\pi j^{v1+1}\frac{A(\tau_1)}{W_2'(\tau_1)}W_2(\tau_1 - h)e^{-j\upsilon_1\phi} \quad (11)$$

where $h = \frac{k}{m}(\rho - a)$. This equation gives the total electric field in an accurate and fast computation way.

C. TE polarization

The TE polarization total electric field is given by :

$$\begin{aligned} E_\rho^{\text{TE}} &= \frac{H_0}{j\omega\varepsilon}\frac{1}{\rho}\times \\ &\sum_{n=-\infty}^{+\infty} nj^{n-1}\{J_n(k\rho) - \frac{J_n'(ka)}{H_n^{(2)'}(ka)}H_n^{(2)}(k\rho)\}e^{-jn\phi} \\ E_\phi^{\text{TE}} &= -\frac{kH_0}{j\omega\varepsilon}\times \\ &\sum_{n=-\infty}^{+\infty} j^n\{J_n'(k\rho) - \frac{J_n'(ka)}{H_n^{(2)'}(ka)}H_n^{(2)'}(k\rho)\}e^{-jn\phi} \end{aligned} \quad (12)$$

The equations (12) can also be simplified by introducing a lit region solution given by the GO and a creeping wave expression in the shadow region.

1) Lit Region: The magnetic field H_z^{TE} is given by:

$$H_z^{\text{TE}} = e^{ik\rho\cos(\phi)} + e^{ika\cos(\alpha)}\sqrt{\frac{\rho_r}{\rho_r + s_r}}e^{-iks_r} \quad (13)$$

The Maxwell's equations are used to obtain the electric field :

$$E_\rho^{\text{TE}} = \frac{1}{j\omega\varepsilon}\frac{1}{\rho}\frac{\partial H_z^{\text{TE}}}{\partial\phi} \quad (14)$$

$$E_\phi^{\text{TE}} = -\frac{1}{j\omega\varepsilon}\frac{\partial H_z^{\text{TE}}}{\partial\rho} \quad (15)$$

2) Shadow Region: The shadow region solution is define through an creeping wave modeling. The total field is the given by:

$$\begin{aligned} E_\rho^{\text{TE}} &= \frac{H_0}{j\omega\varepsilon}\frac{1}{\rho}\times \\ &2\pi\sum_s \upsilon_s' j^{\upsilon_s'-1}\frac{A'(\tau_s')}{\tau_s' W_2(\tau_s')}W_2(\tau_s' - h)\Phi_{\upsilon_s'}(\phi) \\ E_\phi^{\text{TE}} &= -\frac{kH_0}{j\omega\varepsilon}\times \\ &\frac{2\pi}{m}\sum_s j^{\upsilon_s'}\frac{A'(\tau_s')}{\tau_s' W_2(\tau_s')}W_2'(\tau_s' - h)\Phi_{\upsilon_s'}(\phi) \end{aligned} \quad (16)$$

where $\upsilon_s' = ka + m\tau_s'$ and τ_s' verifies:

$$W_2'(\tau_s') = 0 \quad (17)$$

The first derivative Airy's function zeros τ_s' are precisely known and by writing $\tau_s' = -(1.5\ q_s')^{2/3}e^{-i\pi/3}$, it can be shown that q_s' can be tabulated as [12]:

$$q_s' = \frac{\pi}{4}l - \frac{0.12378718}{l} + \frac{0.077576}{l^3} - \frac{0.3890}{l^5} + \frac{4.79}{l^7} \quad (18)$$

where $l = 4s - 3$ and s is an positive integer. The first term of sum (16) gives:

$$\begin{aligned} E_\rho^{\text{TE}} &\simeq \frac{H_0}{j\omega\varepsilon}\frac{1}{\rho}2\pi\upsilon_1' j^{\upsilon_1'}\frac{A'(\tau_1')}{\tau_1' W_2(\tau_1')}W_2(\tau_1' - h)e^{-j\upsilon_1'\phi} \\ E_\phi^{\text{TE}} &\simeq -\frac{kH_0}{j\omega\varepsilon}\frac{2\pi}{m}j^{\upsilon_1'+1}\frac{A'(\tau_1')}{\tau_1' W_2(\tau_1')}W_2'(\tau_1' - h)e^{-j\upsilon_1'\phi} \end{aligned} \tag{19}$$

In the case of a PEC cylinder, it can shown that $\tau_1' = 0.5094 - 0.8823j$.

D. Dielectric Generalization

The model developed above can easily been modified for the scattering of a plane wave by a dielectric cylinder. The GO equations (7) and (13) are modified by introducing a reflection coefficient [11]. The creeping wave solution (11) and (11) are adapted by introducing new values of τ_1 and τ_1'. For TM polarization, it can be shown that τ_1 verifies:

$$W_2'(\tau_1) - qW_2(\tau_1) = 0 \tag{20}$$

and for TE polarization, τ_1' verifies:

$$qW_2'(\tau_1) - W_2(\tau_1) = 0 \tag{21}$$

where $q = m\sqrt{\varepsilon_r}$. It can shown that the PEC solution is an excellent approximation of a dielectric cylinder filled with the electric properties of the human body at 60 GHz. For TE polarization, equation (21) has to be used.

III. Numerical Simulations

In this section, the exact solution of the boundary problem defined by equation (4) for TM mode and (12) for TE mode are used even if the calculation is time-consuming to valid our model given by the combination of the GO result and the creeping wave solution. Comparison is shown in Fig. 2.

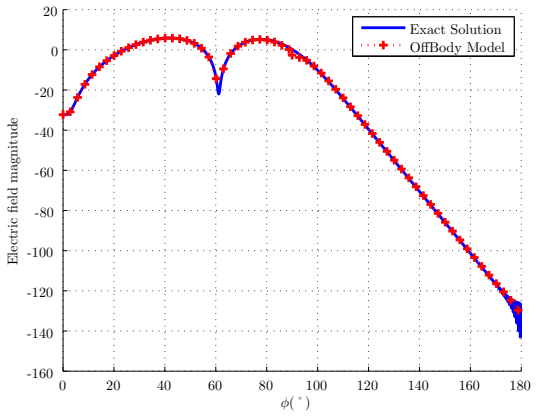

Fig. 2. TM mode. Comparison between the exact solution eq. (4) and the two-components model eq. (7) and (11) for a PEC cylinder with $f = 60$ GHz, $a = 0.2$ m and $\Delta r = 5$ mm.

As it is shown, the Off-Body model shows an perfect agreement with the exact solution. A little deviation can be observed around the shadow boundary ($\phi = 90^\circ$).

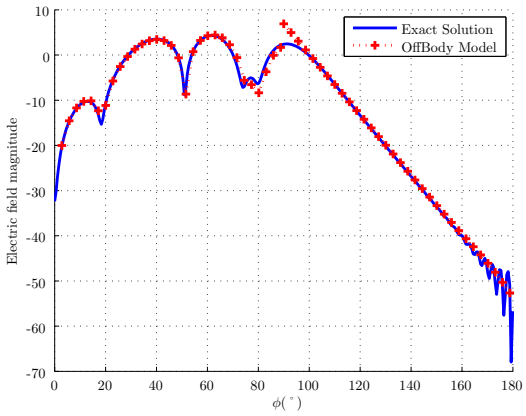

Fig. 3. TM mode. Comparison between the exact solution eq. (12) and the two-components model eq. (13) and (16) for a PEC cylinder with $f = 60$ GHz, $a = 0.2$ m and $\Delta r = 5$ mm.

The TE polarization is studied in Fig. 3.

The Off-Body model shows excellent agreement with the exact solution. The deviation around the shadow boundary ($\phi = 90^\circ$) is spread on a few degrees.

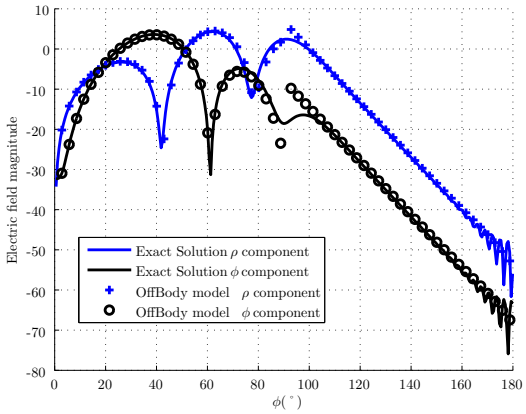

Fig. 4. TM mode. Comparison for ρ and ϕ component between the exact solution eq. (12) and the two-components model eq. (13) and (16) for a PEC cylinder with $f = 60$ GHz, $a = 0.2$ m and $\Delta r = 5$ mm.

As shown in Fig. 4, both ρ and ϕ component of the electric field are perfectly represented by the Off-Body model.

IV. Experimental Comparison

A. Experimental set-up

The creeping wave model have been verified by conducting measurements using an *Agilent E8361C VNA* in an anechoic chamber. V-band horn antennas were used with a beamwidth of 10° and a gain of 20 dBi. The horn antennas have a size of 3 cm x 2.3 cm.

As can be observed in Fig. 5, the Tx horn antenna is located far from the cylinder to obtain a plane wave illumination. The Rx horn antenna is located tangentially to the cylinder

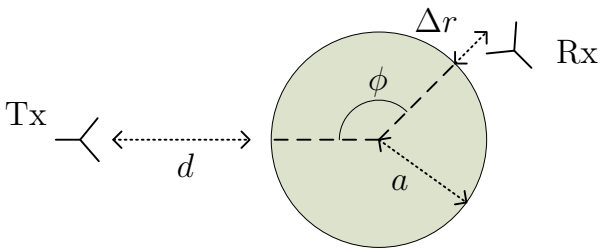

Fig. 5. Experimental set-up

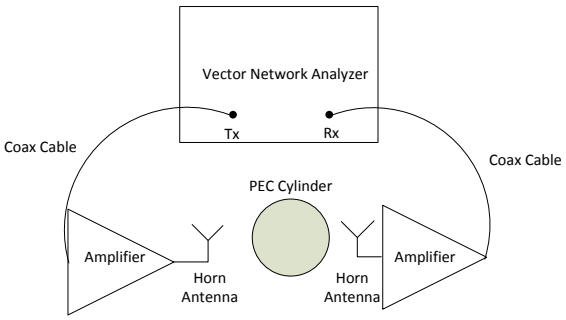

Fig. 6. TM mode Experimental set-up

to maximize the amount of power received from the creeping wave. The distance Δr is defined from the middle of the horn antenna. The parameters take the following values: The

TABLE I
SPATIAL PARAMETERS VALUES

Symbol	Value
a	0.2 m
d	1.92 m
ϕ	90 ° - 180 °
Angular Step $\Delta\phi$	5 ° (or 10 °)

cylinder has a height of 1.2 m and the horn antennas are sited at the middle height. To discriminate the time of arrival of the creeping wave between two spatial positions with $\Delta\phi = 10\,^{\circ}$, a 10 GHz bandwidth is selected.

TABLE II
VNA FREQUENCY PARAMETERS VALUES

Symbol	Value
f_{start}	50 GHz
f_{stop}	60 GHz
f_{step}	66.67 MHz
IFbandwidth	1 Hz
Averaging parameter	1024

The frequency step is chosen in a such way that the length of the signal impulse response is 0.015 μs which is equivalent to a travel of 4.5 m which is sufficient to get the needed paths. The IFbandwidth and the averaging parameter are chosen to have the highest dynamic range possible. The measurement setp-up is presented in Fig. 6.

The TM mode needs a higher dynamic range than the TE mode. In consequence, an amplifier has been put at the receiver side. To reduce the calibration noise and the saturation risks of the amplifier, this latter has been removed for the TE mode.

The coaxial cables have about 6 dB/m losses. To avoid the need of long distance cables and optimize the received power, the VNA has been put inside the anechoic chamber and covered by absorbing material.

B. Experimental Path-Loss

As shown by [10], even if the measurements have been done in an anechoic chamber, some reflected waves can distort the results, especially while dealing with low power measurements. Time gating has been performed to increase the dynamic range and precision of the presented results. Time gating is centered on the predicted time of arrival of the creeping wave.

1) TM polarization: The measurements made with the VNA are compared with (11) for $\Delta r = 15$ mm. The representation of the measurements has been done by normalizing the theoretical path-losses by imposing that the model received power at $\phi = 90\,^{\circ}$ is equal to the measurements.

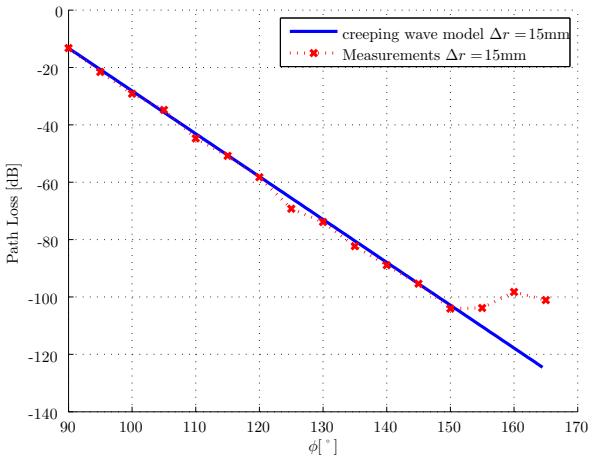

Fig. 7. Comparison between the TM creeping wave model and the measurements for a value of $\Delta r = 15$ mm with $f = 55$ GHz

As can be observed in Fig. 7, the model fits with the measurements although after $\phi = 150\,^{\circ}$ the noise floor is reached and the measurements are no longer valid.

2) TE polarization: To compare the results of the TE mode creeping wave, (16) is used. The theoretical model power is normalized thanks to the first measurement. In fact, only the

ρ polarization of the electric field was measured because of the horn antenna position. Equation (16) is still valid noting that $E_{\phi}^{\mathrm{TE}} \ll E_{\rho}^{\mathrm{TE}}$. The comparison between theoretical and experimental results has been done for a value of $\Delta r = 6.5$ mm.

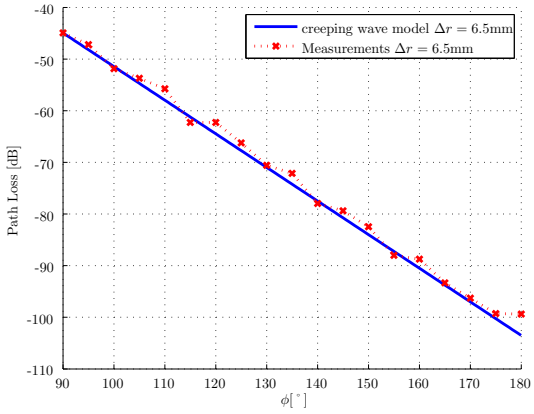

Fig. 8. Comparison between the TE creeping wave model and the measurements for a value of $\Delta r = 6.5$ mm with $f = 55$ GHz

As can be seen in Fig. 8, the dynamic range of the measurements is better than for TM modes and the angular measurement range is then larger. Fig. 8 shows that between $\phi = 90^\circ$ and $\phi = 180^\circ$, the path-loss is linear in dB and the measurements fit with (16).

V. Conclusion

This paper investigates the scattering problem of a plane by a PEC cylinder. The solution developed improves the time of calculation. The propagation model is presented for both TE and TM polarizations. This model is based on a geometrical optics solution in the lit region and a creeping wave formulation in the shadow region. A note is also given for the dielectric cylinder case generalization.

Numerical simulations have been done to compare the model and the exact solution of the boundary problem. It is also be shown that each component of the electric field can be calculated independently.

An experimental validation has been done for both TM and TE modes on a PEC cylinder in an anechoic chamber. The creeping wave path loss shows perfect agreement with the model developed in this paper. The path loss obtained on a PEC cylinder is lower that on a human body but those solutions can easily been generalized in the case of a dielectric cylinder.

Acknowledgement

The authors would like to thank Prof. Bernard Huart, Dr. Reda Mohellab and Antoine Khy from Telecom ParisTech for their helpful advises.

References

[1] N. Guo and R. C. Qiu and S. Mo and K. Takahashi, *60-GHz Millimeter-Wave Radio: Principle, Technology, and New Results*, Eurasip Journal on Wireless Communications and Networking, 2007.

[2] S. Alipour and F. Parvaresh and H. Ghajari and D. F. Kimball, *Propagation Characteristics for a 60 GHz Wireless Body Area Network (WBAN)*, The 2010 Military Communications Conference, 2010.

[3] S. L. Cotton, *A simulated study of co-channel inter-BAN interference at 2.45 GHz and 60 GHz*, Wireless Technology Conference (EuWIT), 2010.

[4] C. A. Balanis, *Advanced Engineering Electromagnetics*, Wiley, 1989.

[5] M. Abramowitz and I. Stegun, *Handbook of Mathematical Functions with Formulas, Graphs, and Mathematical Tables*, Dover Publications, 1964.

[6] P. H. Pathak and W. D. Burnside and R. J. Marhefka, *A uniform GTD analysis of the diffraction of electromagnetic waves by a smooth convex surface*, IEEE Transactions on Antennas and Propagation, 28, pp. 631-642, Sep. 1980.

[7] , P. H. Pathak and N. Wang and W. D. Burnside and R. G. Kouyoumijan, *A uniform GTD solution for the radiation from sources on a convex surface*, IEEE Transactions on Antennas and Propagation, year = 1981.

[8] H. H. Syed and J. L. Volakis, *High frequency scattering by a smooth coated cylinder simulated with generalized impedance boundary conditions*, Radio Sciences, 26, 1305-1314, 1991.

[9] P. A. Hasgall and E. Neufeld, M. C. Gosselin and A. Klingenböck and N. Kuster, *IT'IS Database for thermal and electromagnetic parameters of biological tissues*, Version 2.2, July 11th, 2012. www.itis.ethz.ch/database

[10] A. M. Eid and N. Murtaza and J. W. Wallace, *Green's Function Models and Measurements for Body Area Network (BAN) Channels*, Wireless Information Technology and Systems (ICWITS), 2010.

[11] Y. A. Kravtsov and N. Y. Zhu, *Theory of Diffraction : Heuristic Approaches*, Alpha Science, 2010.

[12] V. I. Ivanov, *Tabulation of the Functions of V.A. Fock*, Journal of Mathematical Sciences, 1982.